MOF-Derived Hierarchically Porous Carbon with Exceptional Porosity and Hydrogen Storage Capacity

ARTICLE *in* CHEMISTRY OF MATERIALS · JANUARY 2012

Impact Factor: 8.35 · DOI: 10.1021/cm202554j

CHEMISTRY OF MATERIALS

Article

pubs.acs.org/cm

MOF-Derived Hierarchically Porous Carbon with Exceptional Porosity and Hydrogen Storage Capacity

Seung Jae Yang,[†] Taehoon Kim,[†] Ji Hyuk Im,[†] Yern Seung Kim,[†] Kunsil Lee,[†] Haesol Jung,[†] and Chong Rae Park*,[†]

[†]Carbon Nanomaterials Design Laboratory, Global Research Laboratory, Research Institute of Advanced Materials, and Department of Materials Science and Engineering, Seoul National University, Seoul 151-744, Korea

Supporting Information

ABSTRACT: Highly porous carbon has played an important role in tackling down the energy and environmental problems due to their attractive features such as high specific surface area (SSA), stability, and mass productivity. Especially, the desirable characteristics of the highly porous carbon such as lightweight, fast adsorption/desorption kinetics, and high SSA have attracted extensive attention in the "hydrogen storage" application which is a main bottleneck for the realization of on-board hydrogen fuel cell vehicles. We herein presented porous carbon with hierarchical pore structure derived from highly crystalline metal organic frameworks (denoted as MOF-derived carbon: MDC) without any carbon source and showed it as a promising hydrogen storage adsorbent. MDCs can be fabricated by a simple heat adjustment of MOFs without complicated process and environmental burden. The MDC displayed hierarchical pore structures with high ultramicroporosity, high SSA, and very high total pore volume. Due to its exceptional porosity, MDCs exhibited reversible H_2 storage capacities at certain conditions that were better than those of previously reported porous carbons and MOFs.

KEYWORDS: *hierarchical structures, hydrogen storage, metal−organic frameworks, nanoporous materials, structure−property relationships*

INTRODUCTION

Highly porous carbonaceous materials have played an important role in addressing global environmental pollution problems. They have high surface areas and good thermal and chemical stabilities and may be mass produced.[1−3] The advantageous characteristics of highly porous carbons, including their lightweight properties, fast kinetics, and high surface area, have attracted attention for use in hydrogen storage applications.[2−5]

A simple approach to achieving high H_2 uptake by porous carbon adsorbents is to increase the specific surface area (SSA) of an adsorbent.[6] Numerous synthetic methods have been adopted to create highly porous carbon materials.[7−9] Typical methods include the creation of porous structures via chemical, physical, and catalytic activation processes.[2,10] Efforts have been applied toward identifying possible methods for enhancing the interactions between hydrogen molecules and carbon, thereby increasing H_2 uptake. Particular attention has been paid to the creation of micropores less than 2 nm in diameter, which is proposed to be an effective pore size for strengthening H_2−adsorbent interactions.[6,11] For example, zeolite-templated carbons (ZTCs) have been suggested as possible adsorbent candidates for the high-capacity storage of hydrogen due to their high microporosity and an SSA exceeding 2500 $m^2\ g^{-1}$.[5] The carbide-derived carbons (CDCs) comprise another class of adsorbents that exhibit excellent hydrogen storage properties due to the presence of well-developed ultramicropores with diameters less than 0.7 nm.[4,12] This pore size is approximately twice the kinetic diameter of hydrogen molecules. TiC-based CDCs exhibit the highest hydrogen storage capacity of all CDCs, 3.0 wt % at 1 bar and 77 K, although the materials yield very low H_2 uptake capacities at room temperature.[4,13]

Taken together, these results suggest that a high hydrogen storage capacity at both cryogenic and room temperatures is not solely a function of the ultramicroporosity but is a multivariable function of high SSA, pore volume, and high ultramicroporosity. It is, however, difficult to fabricate or synthesize adsorbents that fulfill such multivariable performance requirements. A recent study reported the fabrication of such an adsorbent by creating mesoporosity in an ultramicroporous carbon adsorbent via formation of hierarchical porous structures with a measurable SSA and a high total pore volume.[14,15] However, this approach sacrificed ultramicroporosity to the detriment of the high hydrogen storage capacity. In this context, the challenge is to fabricate adsorbents with effective porosities on the micro-, meso-, and macropore scales, producing high SSAs and a high total pore volume. These properties are desirable for achieving high-density hydrogen storage materials.

To address these pore characteristics, Xu et al. reported metal organic framework (MOF)-templated microporous carbon in which the interwoven MOF-5 was used as template

Received: August 26, 2011
Revised: January 4, 2012
Published: January 9, 2012

and furfuryl alcohol was selected as carbon precursor.[16,17] The resultant materials displayed a hierarchical porosity with high micropore volume and SSA exhibiting consequently 2.77 wt % of hydrogen storage capacity at 77 K and 1 bar. Unfortunately, this result did not overcome the highest hydrogen storage capacity of CDCs.

Here, we have attempted to fabricate highly porous carbon adsorbents by carbonizing highly crystalline MOFs without any carbon precursors and focused on the detailed characterization of structure reorganization. The products displayed hierarchical pore structures with high ultramicroporosity, high SSA, and one of the highest total pore volume among all porous adsorbents described in the literature.[18−20] The materials exhibited reversible H_2 storage properties that were better than those of previously described porous carbons and MOFs. These results demonstrated that the pore characteristics of MOF-derived carbons (denoted MDCs) are indeed important for the design of high storage capacities in next-generation H_2 adsorbents.

EXPERIMENTAL SECTION

Reagents and Chemicals. Zinc nitrate tetrahydrate (Merck), terephthalic acid (Aldrich), amino-terephthalic acid (Aldrich), naphthalene dicarboxylate (Aldrich), *N,N′*-dimethylformamide (DMF; Daejung, Korea), *N,N′*-diethylformamide (DEF; Merck), and anhydrous chloroform (Aldrich) were used without purification.

Preparation of IRMOF-1, IRMOF-3, and IRMOF-8. *IRMOF-1.* Zinc nitrate tetrahydrate (0.784 g, 3 mmol) and terephthalic acid (0.166 g, 1 mmol) were dissolved in DEF (30 mL) in a vial. The reaction mixture was heated in a furnace at 105 °C for 24 h to yield large cubic crystals of IRMOF-1. The reaction vessel was removed from the furnace and allowed to cool to room temperature. The cubic crystals were repeatedly washed with DMF and anhydrous chloroform, soaked in anhydrous chloroform for 12 h, filtered, and vacuum-dried at pressures less than 10^{-3} Torr at 150 °C for 24 h.

IRMOF-3. Zinc nitrate tetrahydrate (0.784 g, 3 mmol) and aminobenzene dicarboxylate (0.181 g, 1 mmol) were dissolved in DMF (30 mL) in a vial. The reaction mixture was heated in a furnace at 100 °C for 24 h to yield large cubic crystals of IRMOF-3. Other procedures were similar to those described for IRMOF-1.

IRMOF-8. Zinc nitrate tetrahydrate (0.620 g, 2.4 mmol) and naphthalene dicarboxylate (0.060 g, 0.72 mmol) were dissolved in DMF (30 mL) in a vial. The reaction mixture was heated in a furnace at 100 °C for 24 h to yield large cubic crystals of IRMOF-8. Other procedures were similar to those described for IRMOF-1.

Preparation of MDCs. The prepared MOFs were transferred to a tube furnace and were heat-treated at 900 °C under nitrogen with a heating rate of 5 °C min^{-1} to pyrolyze the organic species. After reaching the target temperature, the material was maintained at this temperature for 3 h and then cooled to room temperature.

Characterization. Thermogravimetric analysis (TGA) was conducted under a nitrogen flow with a heating rate of 5 °C min^{-1}, using an SDT Q600 instrument (TA Instruments). Raman spectroscopy was conducted using a T64000 instrument (HORIABA Jobin Yvon). Temperature-programmed desorption (TPD; ASAP2920; Micromeritics)−mass spectroscopy (MS; HPR20; Hiden Analytical) experiments were performed to examine the decomposition process. Powder X-ray diffraction (XRD) was conducted using a D8 Advance (Bruker) diffractometer. Diffractograms were recorded in reflection mode using Ni-filtered CuK_α radiation (λ = 0.154184 nm). Light microscopy (Leica) and scanning electron microscopy (SEM; JSM6700F instrument, JEOL) equipped with energy dispersive spectroscopy (EDS) were used to analyze the product morphology. Transmission electron microscopy (TEM; Tecnai F20, FEI) was employed for microstructure analysis. Photoluminescence (PL; Shimadzu, RF-5301 PC) was carried out for the optical characterization of ZnO nanoparticles.

Gas Sorption Measurements. Gravimetric H_2 adsorption capacities were measured under high-pressure conditions (up to 100 bar) at 298 K using a magnetic suspension microbalance (Rubotherm), as described previously.[21−23] Volumetric H_2 (at 77 and 298 K) and nitrogen adsorption isotherms (at 77 K) up to 1 bar were measured using a Micromeritics ASAP 2020 static volumetric gas adsorption instrument. All sorption isotherms were obtained using ultrahigh purity gases (99.999%). Prior to the sorption analysis, samples (0.1−0.2 g) in the analysis chamber were subject to a vacuum of 10^{-5} Torr at 150 °C for 12 h. The nitrogen adsorption data permitted calculation of the apparent surface areas based on both the BET and the Langmuir equations. The linearized BET model was fit to the microporous MOF data within the relative pressure range $0.001 < P/P_0 < 0.05$, as described.[24] Pore size distributions were determined using the Tarazona nonlocal density functional theory (NLDFT) model assuming cylindrical pore geometry; the NLDFT software is an integral part of the ASAP 2020 instrument. The obtained pore size distribution of the IRMOF-1 using this model was consistent with the crystallographically determined pore size distribution of the IRMOF-1.[22]

RESULTS AND DISCUSSION

The structural reorganization of MOFs to an amorphous carbonaceous species was confirmed by XRD studies. The patterns of the synthesized IRMOF-1 (Figure 1) were identical with those described previously, and the transparent cubic crystals (Figure 1b, inset) revealed the high crystallinity of the product. The crystallinity of IRMOF-1 usually remains unperturbed up to 300 °C, and further temperature increases result in the formation of ZnO@amorphous carbon, as shown in Figure 1b. This process leads to a complete loss of microporosity as well as a significant increase of meso- and macroporosity (Figure S1). After carbonization, all peaks corresponding to ZnO completely disappeared and nothing else was found (Figure 1b), indicating that the obtained carbon was nearly amorphous and lacked long-range three-dimensional order, as was observed in the ultrahigh porous carbon. In general, ultrahigh porous carbon materials consist of randomly oriented defective graphite nanoflakes, and the thickness of the graphite nanoflakes can determine the SSA of the products. To measure the number of carbon sheets arranged as single layers, Dahn et al. proposed the use of an empirical parameter (R), which is defined as the ratio of the height of the (002) peaks to the background.[25] A value of 1 might indicate that almost all carbon present is in the form of nearly single-layered carbon with few stacking along 002 direction.[2,17] The R-value of MDC-1 demonstrated the presence of randomly distributed nearly single-layered carbon sheets, and the MDC-1 appeared to consist of highly porous carbon.

The thermal decomposition of IRMOF-1 crystals was investigated using temperature-programmed desorption (TPD)−mass spectroscopy (MS). The thermal conductivity detection (TCD) signals indicated two main structural changes in the IRMOF-1 during carbonization (Figure 2), corresponding to the thermal gravimetrical result (Figure S3). The first structural change was mainly due to the evolution of CO_2, CO, and benzene, which originated from the decomposition of the ligand molecules. During the first structural change, the materials were composed of ZnO and carbonaceous materials. The second change began at 750 °C and ended abruptly within 230 min (the temperature was maintained at 900 °C for 50 min). This change was accompanied by the evaporation of CO_2, CO, and slight amounts of Zn and ZnO. This transition corresponded to the reduction of ZnO in the presence of a carbonaceous material because ZnO generally decomposes at much higher temperatures. The carbonaceous materials deoxidized ZnO and then evaporated to form mainly CO and CO_2. Simultaneously, the reduced Zn metal (boiling point: 908 °C) was easily

dx.doi.org/10.1021/cm202554j | *Chem. Mater.* 2012, 24, 464−470

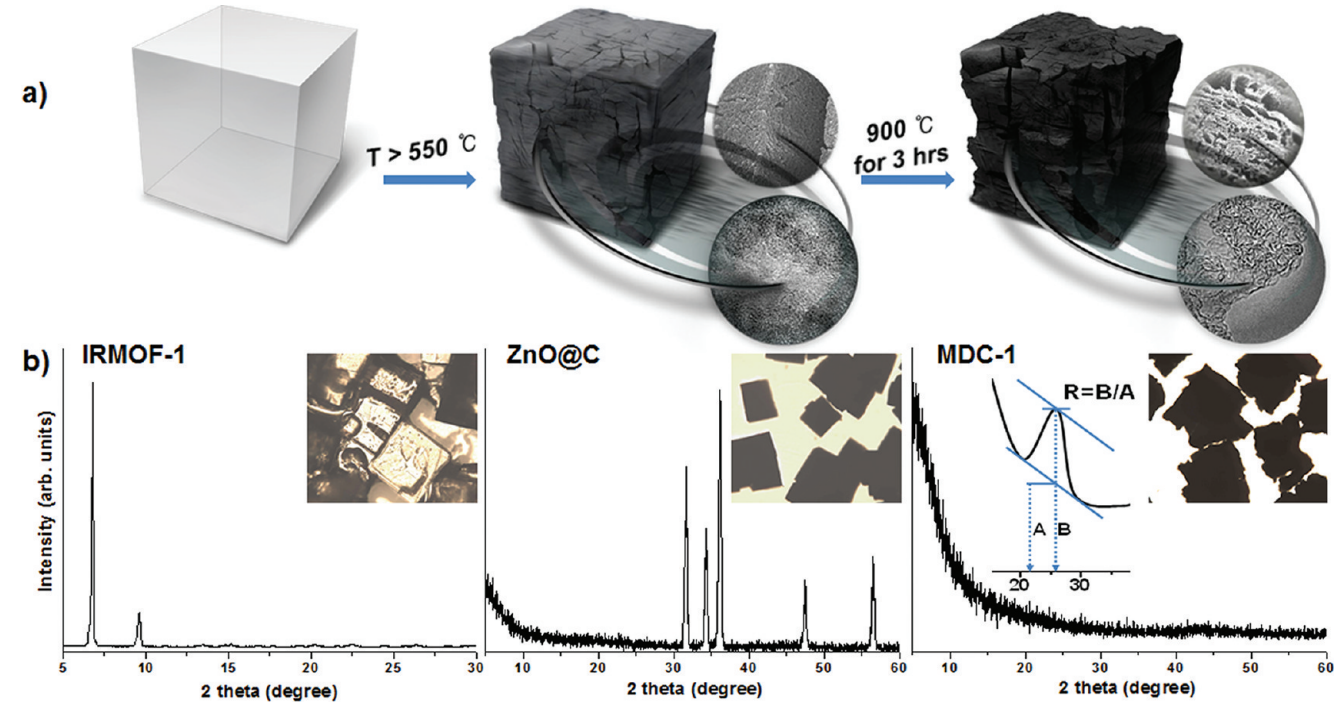

Figure 1. Structural changes of IRMOF-1 with heat-treatment to yield MDC-1: (a) schematic view and (b) PXRD patterns with corresponding optical micrographs.

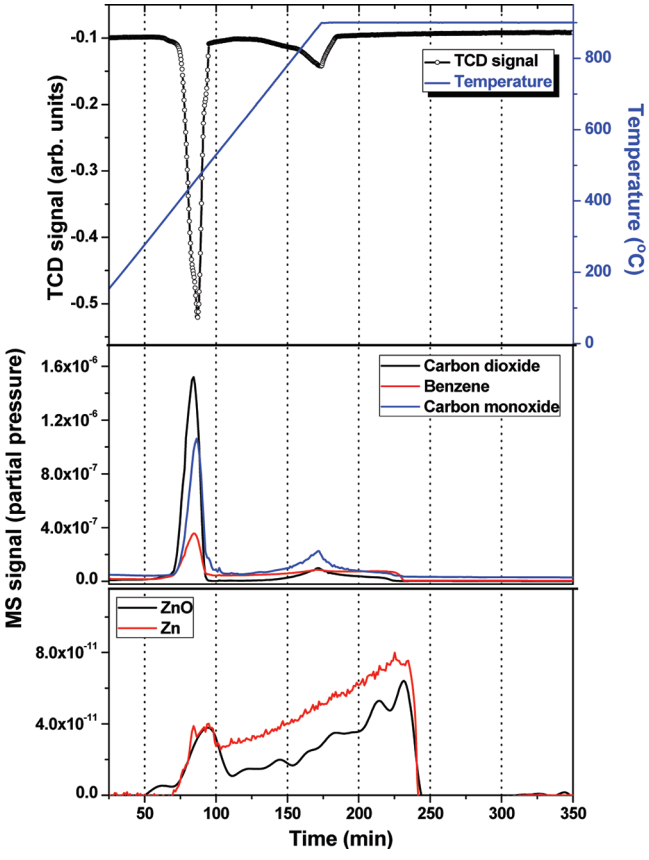

Figure 2. TCD and mass spectroscopy signals of the gas products of the decomposition of IRMOF-1.

vaporized with heating at 900 °C for 50 min, as demonstrated by the MS profile and the XRD results (Figure S2). The nearly 54% of organic species in IRMOF-1 was transferred into the carbon (Figure S3). A previous study suggested a possible mechanism whereby the Zn-based MOFs decomposed.[16,17] These TPD-MS results suggested the more detailed carbonization process of Zn-based MOFs. Further detailed structure reorganization and pore evolution process are investigated by SEM, TEM, Raman spectroscopy, photoluminescence, nitrogen adsorption, and XRD (see the Supporting Information).

SEM images indicated that MDC-1 retained the cubic morphology of IRMOF-1, even after high-temperature carbonization (Figure 3). However, high-magnification images revealed a wide range of pore sizes, from several micrometers to nanometers, compared with the defect-free smooth surface of IRMOF-1 (inset of Figure 3a) and the typical smooth surface of ZTCs, CDC, and MOF-templated carbon.[8,9,16,17] The three-dimensional bicontinuous network of nanosized carbon particles with grain sizes of 10 nm yielded a hierarchical porosity. HRTEM images (Figure 3f) further supported the high porosity of the product. Due to the ultramicroporosity, the material was translucent and was formed from fragile ultrathin one- or two-layer graphene, consistent with the XRD results.[26]

The surface textural characteristics of the MDCs were quantified by measuring cryogenic N_2 sorption curves (Figure 4a for MDC-1, Figure S8 for MDC-3 and MDC-8). In conjunction with SEM images, the N_2 isotherms of MDCs clearly supported the evolving development of a hierarchical pore system from typical monosized microporous IRMOFs. The MDC-1 isotherm exhibited combined characteristics of type I/II/IV materials. A steep increase was observed at low pressures, followed by a moderate slope at intermediate pressures accompanied by a desorption hysteresis. At high pressures, the isotherm increased, indicating the combined effects of the micropores, mesopores, and macropores in the MDC-1, consistent with the SEM and TEM results. A semilogarithmic plot of the nitrogen isotherms differentiated the sorption behaviors of the various samples, and the initial adsorption at low

dx.doi.org/10.1021/cm202554j | *Chem. Mater.* 2012, 24, 464–470

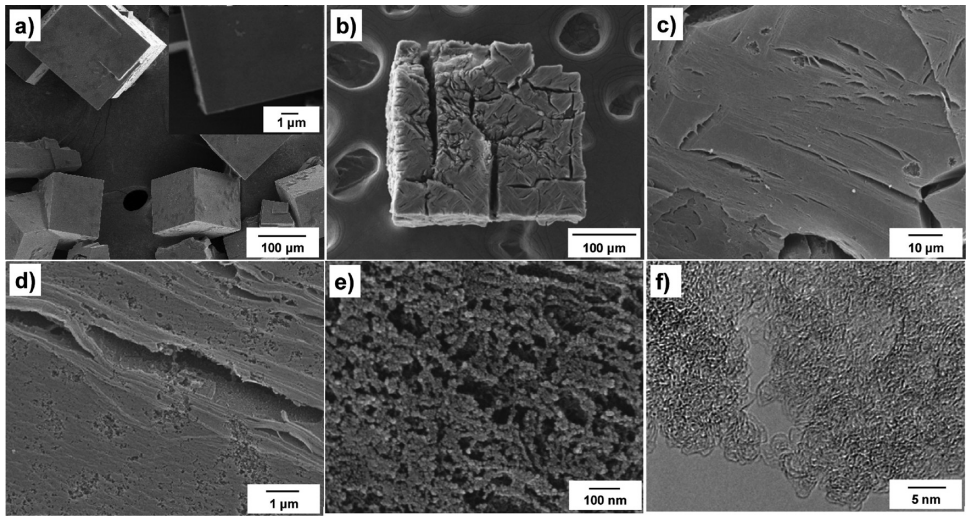

Figure 3. SEM micrographs of (a) IRMOF-1 and (b, c, d, and e) MDC-1. (f) HR-TEM micrograph of MDC-1.

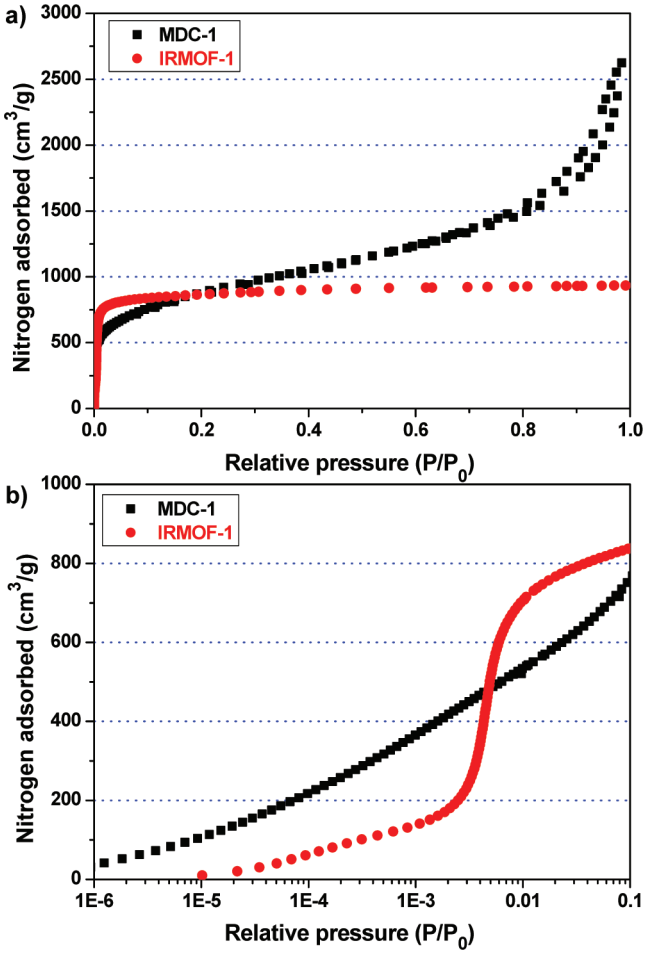

Figure 4. (a) Nitrogen adsorption isotherms of IRMOF-1 and MDC-1. (b) Semilogarithmic plots of nitrogen adsorption isotherms.

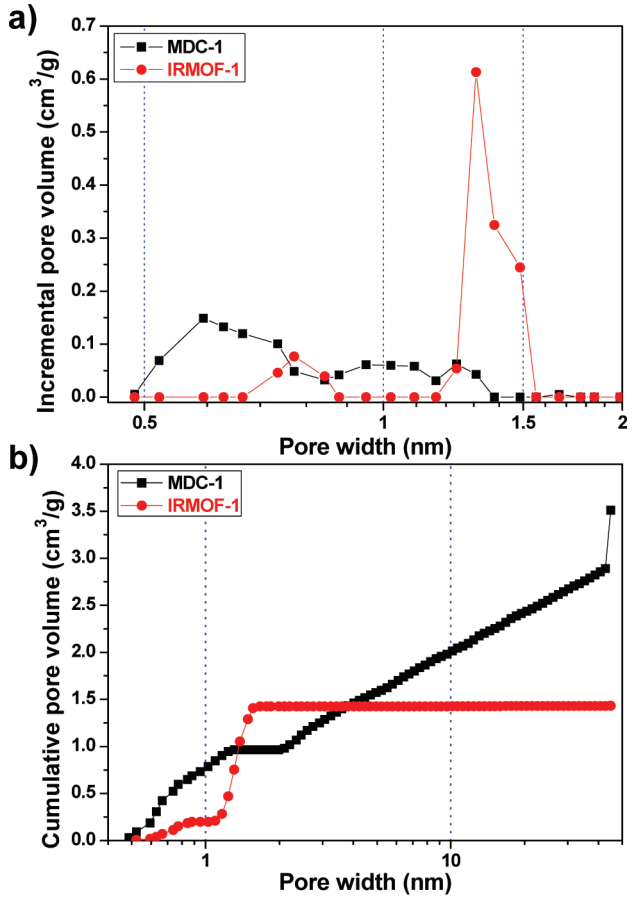

Figure 5. (a) Pore size distribution in the micropore region and (b) cumulative pore volume derived using non local density function theory (NLDFT).

pressures suggested that the MDC-1 micropores were smaller than those of IRMOF-1 (Figure 4b). The pore-size distributions (PSD) derived using nonlocal density functional theory (NLDFT) in the micropore region (Figure 5a).[27,28] The PSD of IRMOF-1 showed a narrow pore size centered at 1.3 nm with negligible mesopores, typical of the IRMOF-1 surface morphology. Compared with these results, the MDC-1 displayed an extremely high ultramicroporosity (0.63 $cm^3\ g^{-1}$; see Table 1) with high meso- and macroporosities (Figure 5b). Furthermore, the N_2 uptake in MDC-1 reached 2625 $cm^3\ g^{-1}$. This uptake is comparable to those reported previously for other ultrahigh porous materials.[18−20,29] The N_2 uptake established a new benchmark for one of the highest total pore volume, exceeding 4 $cm^3\ g^{-1}$ (determined at P/P_0 = 0.98). Carbonization of the

dx.doi.org/10.1021/cm202554j | Chem. Mater. 2012, 24, 464−470

Table 1. Textural Characteristics of the Products

	BET SSA ($m^2\ g^{-1}$)	Langmuir SSA ($m^2\ g^{-1}$)	total pore volume ($cm^3\ g^{-1}$)[a]	ultramicropore volume (<0.8 nm) ($cm^3\ g^{-1}$)[b]	micropore volume ($cm^3\ g^{-1}$)[b]	meso+macro pore volume ($cm^3\ g^{-1}$)[c]
IRMOF-1	3447	3801	1.45	0.17	1.40	0.05
IRMOF-3	2351	2507	0.90	0.18	0.90	0
IRMOF-8	1735	1908	0.69	0.40	0.69	0
MDC-1	3174	5004	4.06	0.63	1.01	3.05
MDC-3	1678	2154	2.01	0.49	0.66	1.35
MDC-8	1978	2719	1.92	0.54	0.78	1.14

[a]The pore volume is calculated at a relative pressure of 0.98. [b]Ultramicropore and micropore volumes are calculated by NLDFT. [c]Meso- and macropore volumes are determined by subtracting the micropore volume from the total pore volume.

IRMOFs proceeded with reorganization into a hierarchical porous structure with ultramicro-, micro-, meso-, and macropores, which displayed a high pore volume (Table 1).

The H_2 adsorption isotherms of the synthesized IRMOFs and MDCs, measured at 1 bar and liquid nitrogen temperature (77 K) by the volumetric method, are shown in Figure 6a.

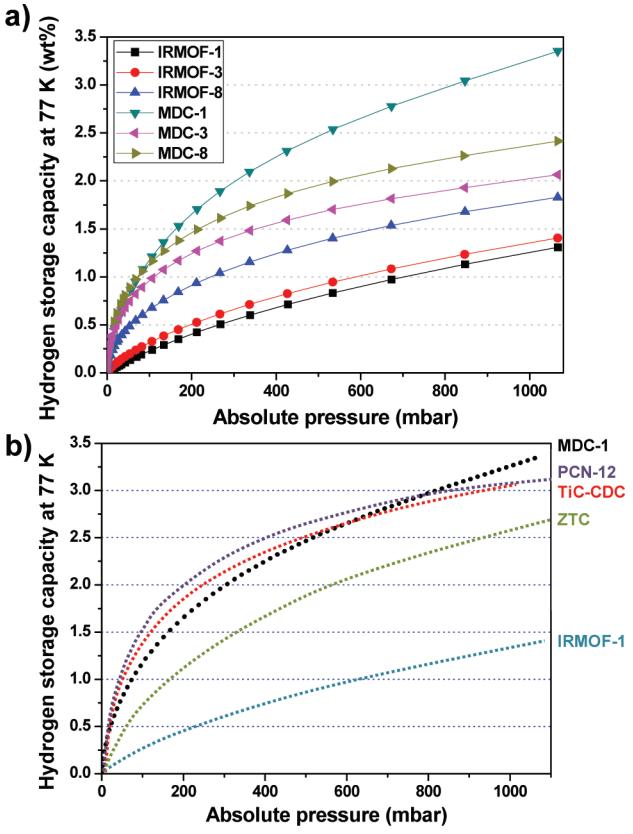

Figure 6. Hydrogen storage capacity at 77 K and 1 bar of (a) the products and (b) the benchmark materials are shown for comparison.

Compared with the MOFs, the corresponding MDCs stored 30% more hydrogen under identical conditions. It is particularly noteworthy that remarkable 2.5-fold and 1.75-fold increases in H_2 uptake were measured for the MDC-1 and -3 materials, respectively. The rates of increase were explained in terms of the textural characteristics of the IRMOFs. The obtained IRMOF-1, -3, and -8 were microporous materials, but only IRMOF-8 included a large degree of ultramicroporosity (Figure S10). Therefore, carbonization did not significantly influence the development of ultramicroporosity in IRMOF-8. Because ultramicroporosity was strongly correlated with the H_2 storage capacity in the limit of coverage experimentally confirmed by previous studies,[2,4,12] the development of ultramicroporosity significantly affected H_2 storage capacities at lower pressures as shown in Figure S6.[4] The relationships demonstrated that a smaller-sized pore exerts a stronger influence on the H_2 storage capacity at 77 K and 1 bar.

The excellent H_2 storage performance of MDCs was compared with the capacities of those benchmark microporous materials, described in the literature, that yielded the best known performance under identical conditions (Table 2).[4,30−33]

Table 2. Hydrogen Uptakes of the Most Representative Adsorbents (MOFs, Porous Carbon) at 77 K and 1 bar, Measured Volumetrically

material	uptake (wt%)	ref	material	uptake (wt%)	ref
MDC-1	3.25	this work	PCN-12	3.05	30
MDC-3	2.1	this work	SNU-5	2.87	32
MDC-8	2.41	this work	Ti-CDC	3.0	4
IRMOF-1	1.3	this work 31,	ZTC	2.6	15
IRMOF-3	1.4	this work 31,			
IRMOF-8	1.9	this work			

In particular, the 3.25 wt % uptake of MDC-1 at 77 K and 1 bar exceeded that of the benchmark materials and surpassed the performance of all other materials characterized to date.

To further elucidate the mechanism underlying the H_2 storage capacity of MDC-1, the H_2 adsorption isotherms of the benchmark materials were superimposed, as shown in Figure 6b.[4,30−33] For the cases of PCN-12 and TiC-CDC, the initial H_2 uptake levels were higher than those of MDC-1 due to their higher ultramicroporosity. Near 1 bar, however, the H_2 capacity of MDC-1 exceeded the capacities of benchmark materials. This material provided a steady increase in H_2 adsorption at 1 bar, whereas the H_2 adsorption properties of the benchmark materials were nearly saturated. This behavior could be explained by the hierarchical pore characteristics of MDC-1 because the porosity of the benchmark materials was almost entirely due to ultramicroporosity. The steady increase in H_2 adsorption of MDC-1 indicated that higher uptakes were expected at higher pressures. Although the mechanism by which hydrogen is stored in the hierarchically porous texture requires further investigation, the ultramicro-/micro-/meso-/macro porosity of the MDCs contributed synergistically to the hydrogen storage performance at both low and high pressures.

High-pressure H_2 storage capacities were achieved and measured using a gravimetric instrument at room temperature (Figure 7a). The H_2 uptakes at 1 bar were comparable with those evaluated by volumetric instruments (Figure S11). At 100 bar and 298 K, IRMOF-1 and MDC-1 exhibited, respectively, 0.45 and 0.94 wt %

dx.doi.org/10.1021/cm202554j | Chem. Mater. 2012, 24, 464−470

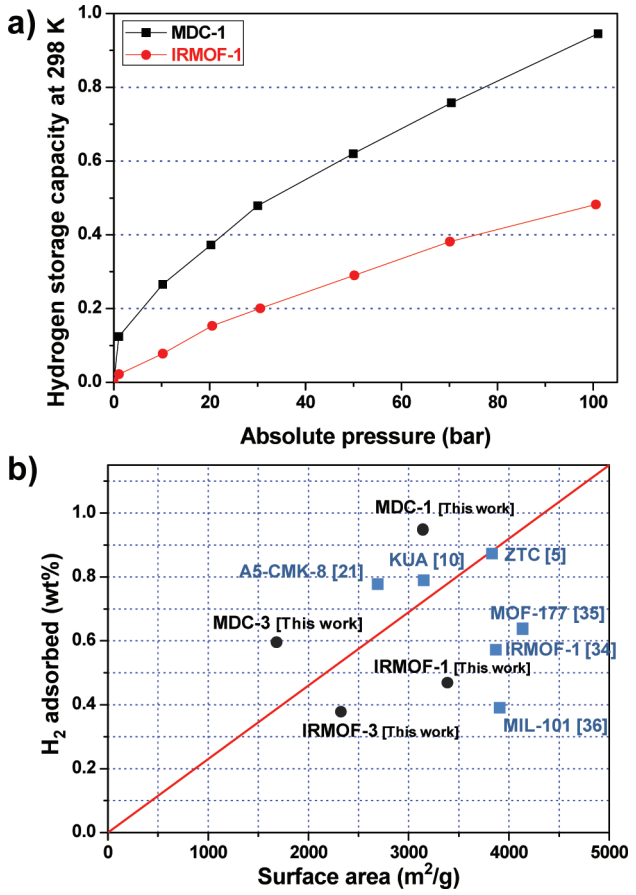

Figure 7. (a) Hydrogen storage capacity at 298 K and 100 bar of IRMOF-1 and MDC-1. (b) Hydrogen adsorption capacities at 298 K and 100 bar of various ultrahigh porous carbons and MOFs plotted as a function of the specific surface area. The slope of the curve was 0.23×10^{-3} wt% m^{-2} g.

H_2 storage capacities. The highest ratio increase (a factor of 5) was observed at 1 bar, indicating that a high ultramicroporosity in MDC-1 led to the efficient storage of H_2 at low pressures. Figure 7b compares the H_2 storage capacities of the synthesized materials at 100 bar and 298 K to the storage capacities of porous carbons and MOFs.[5,10,21,34−36] A linear relationship between H_2 uptake and the specific surface area was first described by Panella et al., who measured a slope of 0.23×10^{-3} wt% m^{-2} g.[6] Although all tested materials were microporous adsorbents, the uptakes of MOFs fell below the line, and the uptakes of the activated carbons fell above the line. This observation supports the assertion that MOFs do not effectively adsorb hydrogen molecules at room temperature due to the large pore size. The MDCs showed exceptionally high H_2 uptakes per specific surface area (0.14, 0.23, 0.25, 0.28, 0.29, and 0.35×10^{-3} wt% m^{-2} g for IRMOF-1, ZTC, KUA-5, A5-CMK-8, MDC-1, and MDC-3, respectively), and MDC-1 surpassed the performance of physisorptive H_2 storage materials at room temperature. The high H_2 storage capacities of MDCs at room temperature might be mainly due to the significantly developed ultramicroporosity, which was supported by theoretical approaches.[11,37] Further, these results highlighted the suitability of the pore textural characteristics of MDCs for H_2 storage at 77 and 298 K over a wide range of pressures.

CONCLUSIONS

In summary, we describe an easy method for preparing hierarchical porous carbon materials from MOFs simply by adjusting the heat treatment without the need for complicated processes or an environmental burden and systematically investigate the carbonizing process with using various characterization tools. The crystalline MOFs reorganized into aggregates of ultramicroporous carbon nanoparticles and retained the pristine cubic morphology during the carbonization process. The MDCs presented a wide range of pore size and volume (up to 4 cm^3 g^{-1}) relative to the properties of previously described porous materials. In particular, the unique hierarchical pore system with a high overall porosity exhibited exceptional H_2 storage capacities at 77 K (1 bar) and 298 K (100 bar), which surpassed the properties of all known physisorptive materials.

ASSOCIATED CONTENT

Supporting Information

TGA, EDS, PXRD, Raman spectroscopy, nitrogen adsorption isotherm, photoluminescence, SEM, and TEM data to elucidate the carbonizing process of MOF. Further detailed information for IRMOF-3, IRMOF-8, MDC-3, and MDC-8. This material is available free of charge via the Internet at http://pubs.acs.org.

AUTHOR INFORMATION

Corresponding Author

*Phone: (+82) 2-880-8030. Fax: (+82) 2-885-1748. E-mail: crpark@snu.ac.kr.

ACKNOWLEDGMENTS

This work was supported by a National Research Foundation of Korea (NRF) grant funded by the Korea government (MEST) [No. 2011-0029865].

REFERENCES

(1) Hartmann, M.; Vinu, A.; Chandrasekar, G. *Chem. Mater.* **2005**, *17*, 829.
(2) Wang, H. L.; Gao, Q. M.; Hu, J. *J. Am. Chem. Soc.* **2009**, *131*, 7016.
(3) Hu, B.; Wang, K.; Wu, L. H.; Yu, S. H.; Antonietti, M.; Titirici, M. M. *Adv. Mater.* **2010**, *22*, 813.
(4) Yushin, G.; Dash, R.; Jagiello, J.; Fischer, J. E.; Gogotsi, Y. *Adv. Funct. Mater.* **2006**, *16*, 2288.
(5) Nishihara, H.; Hou, P. X.; Li, L. X.; Ito, M.; Uchiyama, M.; Kaburagi, T.; Ikura, A.; Katamura, J.; Kawarada, T.; Mizuuchi, K.; Kyotani, T. *J. Phys. Chem. C* **2009**, *113*, 3189.
(6) Panella, B.; Hirscher, M.; Roth, S. *Carbon* **2005**, *43*, 2209.
(7) Lee, J.; Kim, J.; Hyeon, T. *Adv. Mater.* **2006**, *18*, 2073.
(8) Gogotsi, Y.; Nikitin, A.; Ye, H. H.; Zhou, W.; Fischer, J. E.; Yi, B.; Foley, H. C.; Barsoum, M. W. *Nat. Mater.* **2003**, *2*, 591.
(9) Alam, N.; Mokaya, R. *Energy Environ. Sci.* **2010**, *3*, 1773.
(10) Jorda-Beneyto, M.; Suarez-Garcia, F.; Lozano-Castello, D.; Cazorla-Amoros, D.; Linares-Solano, A. *Carbon* **2007**, *45*, 293.
(11) Cabria, I.; Lopez, M. J.; Alonso, J. A. *Carbon* **2007**, *45*, 2649.
(12) Gogotsi, Y.; Dash, R. K.; Yushin, G.; Yildirim, T.; Laudisio, G.; Fischer, J. E. *J. Am. Chem. Soc.* **2005**, *127*, 16006.
(13) Gogotsi, Y.; Portet, C.; Osswald, S.; Simmons, J. M.; Yidirim, T.; Laudisio, G.; Fischer, J. E. *Int. J. Hydrogen Energy* **2009**, *34*, 6314.
(14) Kockrick, E.; Schrage, C.; Borchardt, L.; Klein, N.; Rose, M.; Senkovska, I.; Kaskel, S. *Carbon* **2010**, *48*, 1707.
(15) Sevilla, M.; Foulston, R.; Mokaya, R. *Energ. Environ. Sci.* **2010**, *3*, 223.
(16) Liu, B.; Shioyama, H.; Akita, T.; Xu, Q. *J. Am. Chem. Soc.* **2008**, *130*, 5390.

(17) Jiang, H.-L.; Liu, B.; Lan, Y.-Q.; Kuratani, K.; Akita, T.; Shioyama, H.; Zong, F.; Xu, Q. *J. Am. Chem. Soc.* **2011**, *133*, 11854.
(18) Fan, W.; Snyder, M. A.; Kumar, S.; Lee, P. S.; Yoo, W. C.; McCormick, A. V.; Penn, R. L.; Stein, A.; Tsapatsis, M. *Nat. Mater.* **2008**, *7*, 984.
(19) Lohe, M. R.; Rose, M.; Kaskel, S. *Chem. Commun.* **2009**, 6056.
(20) Tao, Y. S.; Endo, M.; Kaneko, K. *J. Am. Chem. Soc.* **2009**, *131*, 904.
(21) Choi, M.; Ryoo, R. *J. Mater. Chem.* **2007**, *17*, 4204.
(22) Yang, S. J.; Choi, J. Y.; Chae, H. K.; Cho, J. H.; Nahm, K. S.; Park, C. R. *Chem. Mater.* **2009**, *21*, 1893.
(23) Lan, A. D.; Mukasyan, A. *J. Phys. Chem. B* **2005**, *109*, 16011.
(24) Walton, K. S.; Snurr, R. Q. *J. Am. Chem. Soc.* **2007**, *129*, 8552.
(25) Liu, Y. H.; Xue, J. S.; Zheng, T.; Dahn, J. R. *Carbon* **1996**, *34*, 193.
(26) Kuhn, P.; Forget, A.; Su, D. S.; Thomas, A.; Antonietti, M. *J. Am. Chem. Soc.* **2008**, *130*, 13333.
(27) Portehault, D.; Giordano, C.; Gervais, C.; Senkovska, I.; Kaskel, S.; Sanchez, C.; Antonietti, M. *Adv. Funct. Mater.* **2010**, *20*, 1827.
(28) Yang, S. J.; Cho, J. H.; Lee, K.; Kim, T.; Park, C. R. *Chem. Mater.* **2010**, *22*, 6138.
(29) Furukawa, H.; Ko, N.; Go, Y. B.; Aratani, N.; Choi, S. B.; Choi, E.; Yazaydin, A. O.; Snurr, R. Q.; O'Keeffe, M.; Kim, J.; Yaghi, O. M. *Science* **2010**, *329*, 424.
(30) Wang, X. S.; Ma, S. Q.; Forster, P. M.; Yuan, D. Q.; Eckert, J.; Lopez, J. J.; Murphy, B. J.; Parise, J. B.; Zhou, H. C. *Angew. Chem., Int. Ed.* **2008**, *47*, 7263.
(31) Rowsell, J. L. C.; Yaghi, O. M. *J. Am. Chem. Soc.* **2006**, *128*, 1304.
(32) Lee, Y. G.; Moon, H. R.; Cheon, Y. E.; Suh, M. P. *Angew. Chem., Int. Ed.* **2008**, *47*, 7741.
(33) Yang, Z. X.; Xia, Y. D.; Mokaya, R. *J. Am. Chem. Soc.* **2007**, *129*, 1673.
(34) Kaye, S. S.; Dailly, A.; Yaghi, O. M.; Long, J. R. *J. Am. Chem. Soc.* **2007**, *129*, 14176.
(35) Zacharia, R.; Cossement, D.; Lafi, L.; Chahine, R. *J. Mater. Chem.* **2010**, *20*, 2145.
(36) Latroche, M.; Surble, S.; Serre, C.; Mellot-Draznieks, C.; Llewellyn, P. L.; Lee, J. H.; Chang, J. S.; Jhung, S. H.; Ferey, G. *Angew. Chem., Int. Ed.* **2006**, *45*, 8227.
(37) Patchkovskii, S.; Tse, J. S.; Yurchenko, S. N.; Zhechkov, L.; Heine, T.; Seifert, G. *Proc. Natl. Acad. Sci. U.S.A.* **2005**, *102*, 10439.